Research Article

Journal of Clinical Rheumatology Research

Photocatalytic Degradation of Methylene Blue Dye with Green Zinc Oxide Doped with Nitrogen

Nnodim U. J*, Adogwa A. A, Akpan U. G and Ani I. J

Nigeria.

***Corresponding author**

Uche Jude Nnodim, Nigeria.

Submitted: 08 Jun 2022; **Accepted:** 19 Jun 2022; **Published:** 24 Jun 2022

Citation: *Uche Jude Nnodim. (2022). Photocatalytic Degradation of Methylene Blue Dye with Green Zinc Oxide Doped with Nitrogen. J Clin Rheum Res, 2(1), 59-69.*

Abstract

The non-biodegradability of organic pollutants and their adverse effects on plant and living organisms makes their removal from the environment vital for the preservation of the ecosystem. In this study, Photocatalysis (one of the advanced oxidation processes) was employed for the removal of methylene blue dye (MBD). Phyto-enhanced synthesized Zinc oxide (G.S ZnO) were precipitated from an aqueous solution of zinc nitrate hexahydrate and Papaya leaf extracts. The precipitates were dried at 100 oC for 24 hours, and doped hydrothermally with nitrogen from Urea at different doping ratios (10%, 5% and 2%). Preliminary degradation of MBD with the different compositions of Photocatalyst revealed that 5% G.S N-ZnO had superior photocatalytic capabilities than pure ZnO, 10% G.S N-ZnO, 2% G.S N-ZnO. The effects of solution pH, 5% G.S N-ZnO dosage and initial solution concentration on MBD degradation were studied. An optimum percentage degradation of 83% and 97.5% were observed for pure ZnO and G.S. N-ZnO photocatalyst at a solution pH of 9.0, MB solution concentration of 10 mg/L and photocatalyst of dosage of 100 mg. Scanning Electron Microscope (SEM), X-ray Diffraction (XRD), Brunauer-Emmett-Teller (BET) and Fourier Transform Infrared Spectroscopy (FTIR) were used to study morphology, structural properties, surface area and pore volume, and functional groups of Pure ZnO and 5% G.S N-ZnO. FTIR spectra of the 5% G.S N-ZnO was in the range of 4000-500cm-1, and the ZnO group of G.S N-ZnO was at a low wavenumber. The BET result revealed the surface area of 5% G.S N-ZnO to be 113.3cm2/g which was five times that of pure ZnO. The BET result showed an increase in pore volume and diameter (2.118nm and 0.055cm3/g) of 5% G.S N-ZnO against that of pure ZnO (1.452 nm and 0.010 cm3/g). The shift of the XRD pattern between pure ZnO and 5% G.S N-ZnO affirms the presence of dopants in the crystalline structure of ZnO. The average crystallite sizes of pure ZnO and 5% G.S N-ZnO were 34.7nm and 24.8nm, respectively. The findings from this research revealed that the simultaneous use of green synthesis and doping could further improve the degradation of methylene blue dye compounds in industrial effluents and ultimately increase the efficiency of wastewater treatment processes/systems.

Keywords: Photocatalysis, organic dyes, Advanced Oxidation Process, Doping, Nanoparticles, Green Synthesis

Introduction

Water pollution arising from the discharge of non-biodegradable organic materials from process industries into water bodies poses a threat to the eco-system and mankind. Seventy percent of the earth is made up of water (Matt *et.al,* 2014) and recent projections has revealed that water sources are reducing and water would be a scarce commodity in the future. Therefore, it is imperative that sustainable solutions are developed to address the problem of water pollution caused by organic compounds. Several industries contribute greatly to water pollution and amongst them is the textile industry (Chen *et.al,* 2017) with a lot of effluents containing non-biodegradable dyes. Quantitative and qualitative analysis conducted on textile wastewater in the past revealed that they majorly constitute of persistent organic pollutants (POPs). These POPs are recalcitrant, mutagenic, carcinogenic and most times resistant to biodegradation, physical methods and chemical methods (Lawal *et.al,* 2017). A common type of dye found in textile effluents is Methylene blue (MB). Methylene Blue is a cationic dye used in textile industries for various purposes. It is aromatic in nature and has a molecular formula of C16H18N3S. When ingested into the body system of living organisms, it causes genetic diseases and cancer, and it can also result in death (Ullah et.al, 2017).

Over the years, various methods have been proposed to tackle water pollution by organic pollutants. Among these processes are biological methods also called biodegradation and advanced oxidation processes (AOPs). Advanced oxidation processes were identified as the most efficient, sustainable and economically viable method for degradation of organic pollutants in industrial/municipal wastewater. Advanced Oxidation Processes (AOPs) are of six types and among them, Photocatalysis has been identified as the most suitable option for treating wastewater with high con-

centration of organic pollutants (Silva *et al.* 2020). Photocatalysis is the occurrence of redox reaction in the presence of visible light or ultraviolet light and a Photocatalyst. However, Photocatalysis is not without its own drawbacks and one notable drawback is the difference energy band gap between the photocatalyst and light source (visible light or ultraviolet light). Another drawback is the recombination of electron (e-) and holes pair (h+) in the valence band (Akpan & Hameed, 2009).. These drawbacks made researchers focus on photocatalyst precursors like semiconductor metallic oxide i.e Titanium oxide (TiO_2), Zinc Oxide (ZnO), Tungsten Oxide (WO_3), Iodine (III) oxide (In_2O_3) and Tin Oxide (SnO). After several investigations, ZnO was identified as a suitable photocatalyst precursor because of its light-emitting diodes, good sensor abilities, solar light harvesting and high photo-stability (Ani *et al*. 2018), even though the challenge of electron/hole pair recombination and the energy bandgap difference still exists. This prompted the introduction of doping process into the Photocatalyst preparation stage. Doping is the introduction of impurities into a material's crystalline shape. Recent studies by Nguyen and Marques (2018) revealed that doping a photocatalyst with appropriate impurity material reduces the energy bandgap difference between the photocatalyst and the visible light region, which in turn makes the photocatalyst active in the visible light region. Material impurities such as nitrogen, sulphur atoms, cobalt and graphitic carbon have been identified and explored for doping in recent years.

In recent times, doping of ZnO with nitrogen has gained much attention and several doping methods have been employed. These methods include; thermal evaporation, thermal nitridation (with ammonia precursor for nitrogen) and hydrothermal methods. Among these methods, hydrothermal demonstrated better advantages because of its simplicity, less time consumption, low energy demands and eco-friendliness.

This study presents the synthesis of pure zinc oxide, green nitrogen doped zinc oxide (GS N-ZnO) and the photocatalytic degradation of Methylene blue (MB) dye in synthetic wastewater with GS N-ZnO.

Materials and Methods

Materials and Reagents: Sodium Hydroxide, Zinc nitrate hexahydrate, Urea, Deionized water, Carica papaya leaf. . All reagents and chemicals were purchased and delivered from Sigma Aldrich Chemical Company and were analytical grade. *Carica papaya* (paw-paw) leaf were collected from Minna Niger State, Nigeria, washed with deionized water and stored in an environment with room temperature.

Extraction of extract from *Carica papaya*: 10 g of well ground dried paw-paw leaves was mixed with 100 ml of deionized water in a 250 ml beaker. The mixture was stirred and heated for 30 min and 60 ^{o}C respectively on a heating mantle. After this, the mixture was allowed to cool and the liquid extract was collected and stored in a refrigerator at 4 ^{o}C

Figure 1.0: Extraction of liquid from *Carica papaya leaf*

Synthesis of pure Zinc Oxide (ZnO): 0.7 M of zinc nitrate hexahydrate [Zn(NO3)2.6H2O] prepared and poured into a flat bottom flask containing 30 ml of deionized water, and the mixture was stirred at 50 rpm for 60 min. Drops of 4 M of NaOH was then added intermittently to ensure the precipitation of zinc oxide, and this continued until no further precipitation was observed. The upper region of the flat bottom flask (liquid layer) was then decanted and the bottom region (solid layer) was collected and washed three times with deionized water. The solid precipitates (ZnO) was then oven-dried at 100 oC for 6 h and after this, the weight of dried ZnO was observed to be 9.8g. Dried ZnO was calcined at 350 oC for 2 h in a muffle furnace.

Synthesis of green nitrogen-doped zinc oxide: 0.7 M of zinc nitrate hexahydrate [Zn(NO3)2.6H2O] was poured into a flat bottom flask containing 30 ml of Carica papaya liquid extract and the solution was stirred at 50 rpm for 60 min. The pH of the mixture was adjusted to 12 with aqueous solution of NaOH to ensure the complete precipitation of green zinc oxide particles, and the mass of the particles was observed to be 9.8 g. 1 g of urea and 9.8 g of green zinc oxide was then transferred to a flat bottom flask containing 30 ml of deionized water. The mixture was mixed vigorously at 80 rpm for 6 h and allowed to settle for 30 min. The liquid layer at the upper region was then decanted and the leftover solid was over-dried at 100 oC for 6 h. The resulting solid material (green nitrogen doped zinc oxide) was calcined at 350 oC for 2 h in muffle furnace. The process was then repeated with varying mass of 0.2g to 2g of urea.

Figure 2.0: Synthesis of green synthesized Zinc Oxide (G.S ZnO)

Figure 3.0: Doping of nitrogen on G.S ZnO

Photocatalytic experiment with green nitrogen doped zinc oxide: The performance of the green nitrogen doped zinc oxide was evaluated on the degradation of methylene blue dye compounds in synthetic wastewater. 0.1 g of the photocatalyst was measured and transferred into a flat bottom flask containing 100ml of methylene blue dye solution and the pH of the solution was adjusted to 3 with intermittent drops of aqueous HCl acid. The mixture was first stirred for 30 min inside a cupboard in the absence of visible light to attain adsorption-desorption equilibrium. The mixture was then exposed to sunlight for 3 h for the occurrence of Photocatalysis. Liquid samples of the mixture was withdrawn after every 15 min, centrifuged to obtain a clear solution and then analyzed with a UV spectrophotometer. The spectrum was recorded at 668 nm and a percentage decrease was evaluated with the Equation below.

$$\text{Percentage removal} = Co\text{-}Ct \,/\, Co \times 100 \quad (1)$$

Where Co and Ct are initial concentration and concentration at time t. This procedure was repeated for pH values of 5, 9 and 11 and photocatalyst dosage of 0.2 – 1 g.

Result and discussion

Characterization of the Photocatalyst

Scanning electron microscope (SEM): The SEM technique was used to study the morphology of the pure ZnO and green nitrogen doped ZnO. As shown in Figure I, the SEM micrographs for pure ZnO and green nitrogen doped ZnO were taken at 200 nm. The SEM micrograph of pure ZnO show a network configuration of agglomerated elongated rod-like shapes while the SEM micrograph of green nitrogen doped ZnO revealed a loosed structure of uniformly distributed particles. The increase in surface area in green nitrogen doped ZnO affirms green synthesis had significant effect on the photocatalyst and also suggest that it improves the efficiency of the entire photocatalytic process.

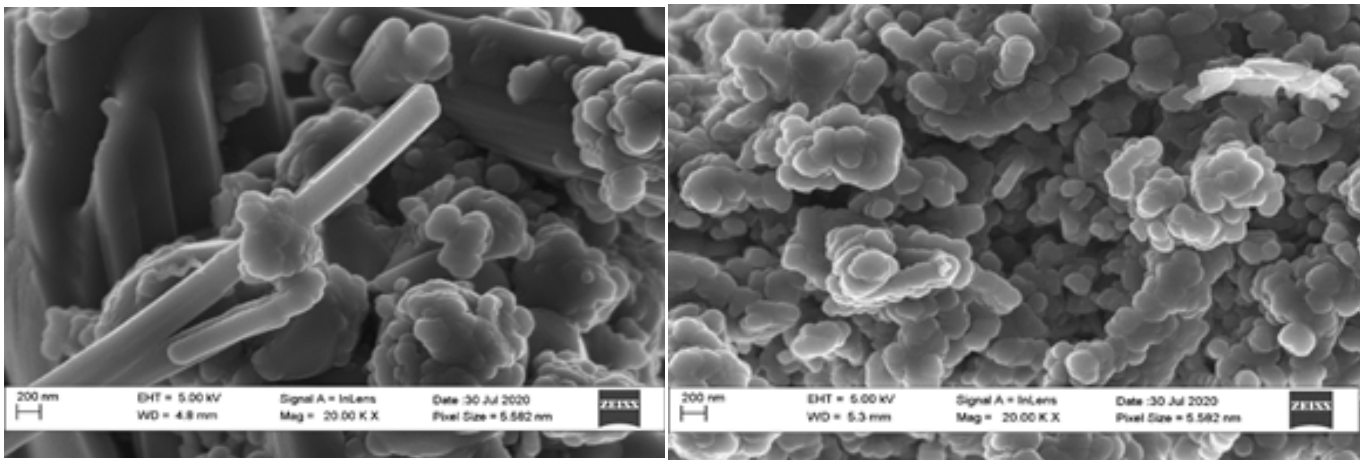

Figure 4.0: SEM Micrograph pf pure ZnO (A) and G.S N-ZnO (B)

Energy dispersive X-ray (EDX): The elemental composition of pure ZnO and green nitrogen doped and their respective weights are presented in the Figure II. Figure II presents two spectra for pure ZnO (A) and green nitrogen doped ZnO (B). It can be observed that sample B has nitrogen presented in minute amount, and this resulted from the low doping ratio during the synthesis of the photocatalyst. The observed peaks of Potassium (K), Sulphur(S), magnesium (Mg) and phosphorus (P) in traces is attributed to surface contamination during the analysis. In addition, the carbon peaks observed are due to the carbon composition of the storage material and the carbon from the precursor for nitrogen (urea).

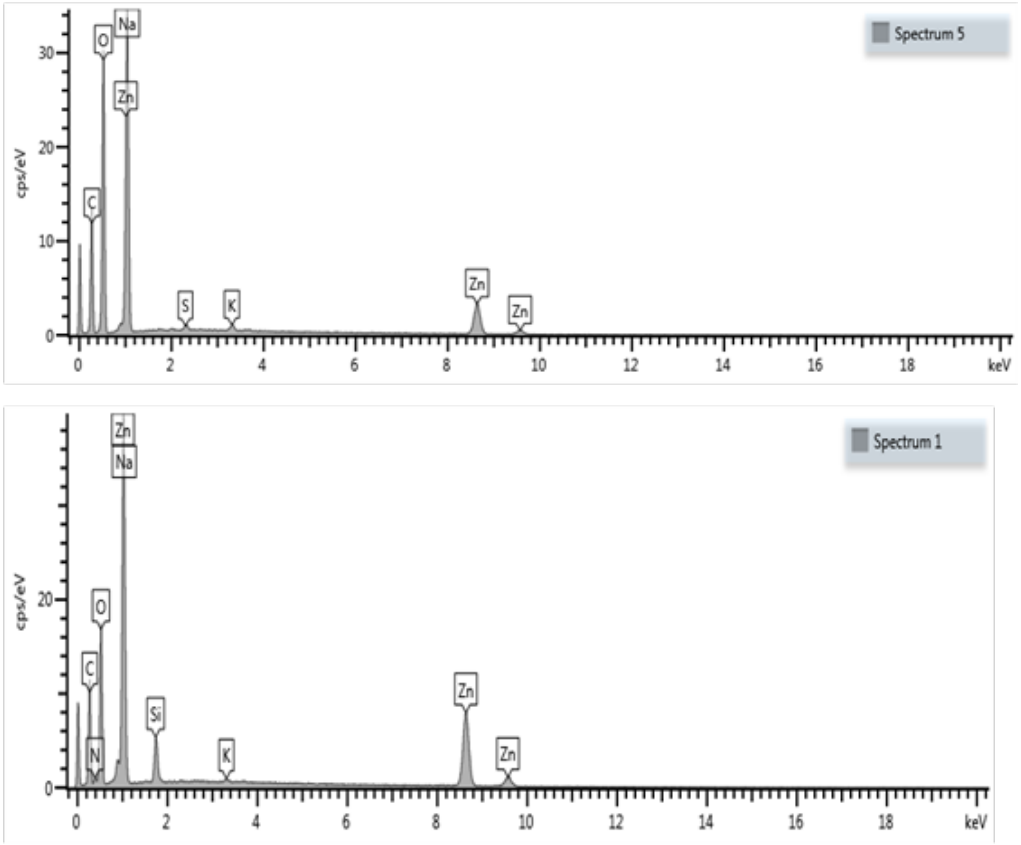

Figure 5.0: EDX spectra of pure ZnO (A) and green nitrogen doped ZnO (B)

Brunauer-Emmett-Teller (BET): The surface area, pore size and pore volume were determined through the BJH Adsorption method of the BET analysis. As presented in Table 1, the surface area, pore size and pore volume of pure ZnO was observed to be lower than that of green nitrogen doped ZnO. This is attributed to the effects of green synthesis on pure zinc oxide. The high surface area, pore diameter and pore volume of green nitrogen doped ZnO led to an increase in percentage degradation of methylene blue dye compounds.

Table 1: BET Summary

Photocatalyst	Pure ZnO	Green N-ZnO
Surface area (m^2/g)	22.27	113.3
Pore diameter (nm)	1.453	2.118
Pore volume (cm^3/g)	0.010	0.055

Fourier-transform infrared spectroscopy (FTIR): The functional groups of pure ZnO and green nitrogen doped ZnO were investigated with the FTIR spectroscopy. The functional groups are revealed in a wave number range frequency range of 4000 – 500 cm-1. As seen on Figure III below, eight peaks were present in the pure ZnO and green nitrogen doped zinc oxide spectra. In Tables 2 and 3, the peaks and their corresponding groups and classes are clearly stated. The third peak (1773.91 cm-1) belongs to N-O stretching confirms the presence of nitrogen arising from doping on the photocatalyst which agrees with a study carried out by Prabakaran (2019).

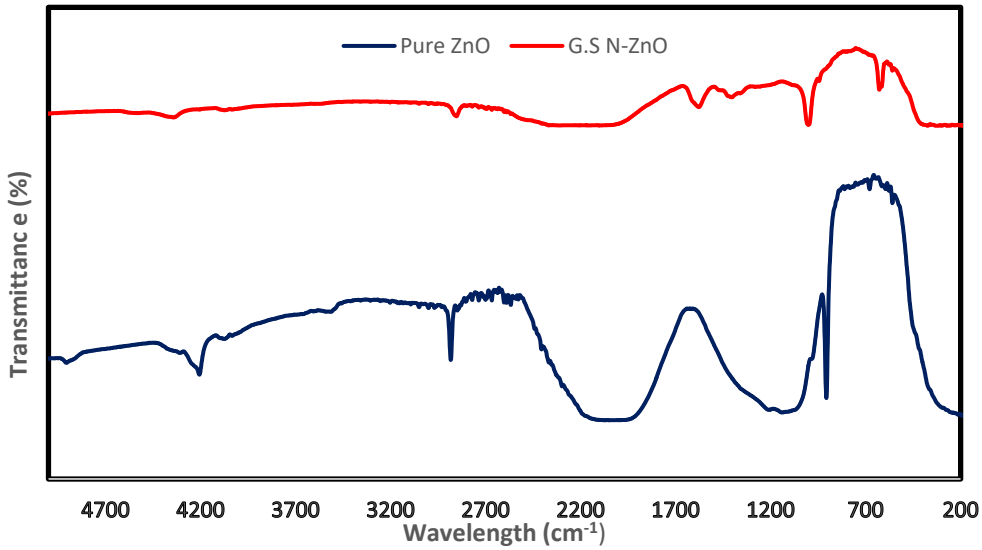

Figure 6.0: FTIR Spectra for pure ZnO and GS N-ZnO

Table 2: Frequency Table for Pure ZnO

Peaks (cm^{-1})	Group	Class
3484.70	O-H stretching	Alcohols
2763.80	C-H stretching	Aldehydes
2426.52	C=O stretching	Carbon dioxide
1788.45	C-H bending	Aromatic
1342.61	S=stretching	Sulphone
834.27	C=H	Alkene

Table 3: Frequency Table for Pure G.S N-ZnO

Peaks (cm^{-1})	Group	Class
2490	D-H stretching	Carbon dioxide
1773.91	C=O stretching	Acid halide
1524.31	N-O stretching	Nitro
1155.73	C-F stretching	Floro
1069.698	S=O stretching	Sulphoxide
881.33	C=C bend	Vinyldene

X-ray Diffraction (XRD): The phase composition, lattice parameter and crystallite size of pure ZnO and green N-doped ZnO were determined from the XRD spectra presented in Figure 4. The 2θ values for Pure ZnO corresponding to diffraction peaks are 31.82, 34.53, 36.25, 47.57, 56.58, 62.94, 68.00, 69.14o and for nitrogen doped ZnO, 2θ values were 31.82, 34.53, 37.25, 47.57, 56.58, 62.94, 68.00, 69.14o. These peaks correspond to the miller index (100), (002), (101), (102), (110), (103) and (112) in that order. This affirms that the hexagonal wurtzite structure of N-doped ZnO (Prabakaran *et al.*, 2019), which agrees with the JCPDS card no 36-1451. On careful examination of the XRD pattern, one can notice a minute shift in the third peak between pure ZnO and Nitrogen doped ZnO. This confirms the presence of nitrogen resulting from doping of urea on pure ZnO. The crystallite sizes of pure ZnO and N-ZnO nanoparticles were calculated with the Bragg's formula as shown in Equation 2

$$D=0.89\lambda/\beta\cos\Theta \quad \text{---------- 2}$$

Where D is the crystallite size of the photocatalyst, λ is the wavelength of the X-ray beam operating system, ß is full width half maximum and Θ is the angle of diffraction. The crystallite size of pure ZnO and green N-doped ZnO were estimated as 34.7nm and 24.8nm.

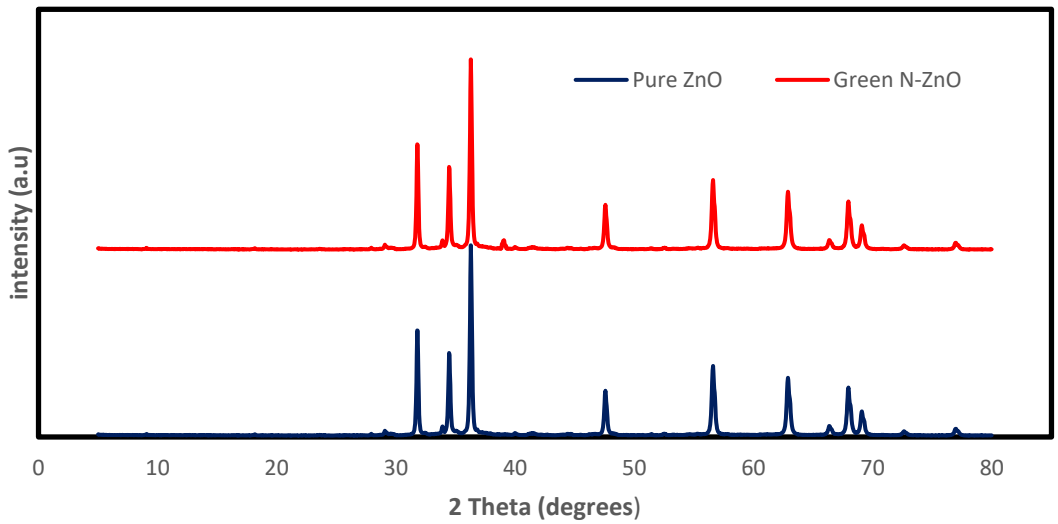

Figure 7.0: XRD spectra for pure ZnO and green N-doped ZnO

Effects of process parameters on degradation of MB dye with green N-ZnO

Effect of solution pH on degradation of MB dye: The pH of the solution plays a significant role in Photocatalysis because the pH of wastewater varies. Therefore it was imperative to study the effects of solution pH on the degradation of methylene blue dye. The pH of MB dye solution was adjusted with sodium hydroxide (NaOH) and hydrochloric acid (HCl). The effect of solution pH was studied at constant initial concentration of 10 mg/L and constant photocatalyst dosage of 100 mg. From Figure 5, degradation of MB dye was observed to be lower at pH of 3 and 5 but higher at pH of 9 and 11. The low degradation of MB dye at pH 3 and 5 is attributed to the force of repulsion between MB and the photocatalyst surface. At $p < 6$, MB exists in a cationic form and the point zero charge of the photocatalyst which was estimated to be 9.3 causes a force of repulsion between both surfaces, which led to reduced adsorption and consequently low degradation of MB dye. However, at pH > 7.7, MB exists in anionic form and this creates an electrostatic attraction between the positively charged photocatalyst surface and MB dye, thus leading to high adsorption of MB on the photocatalyst surface and consequently high degradation (Priya et. al 2015)

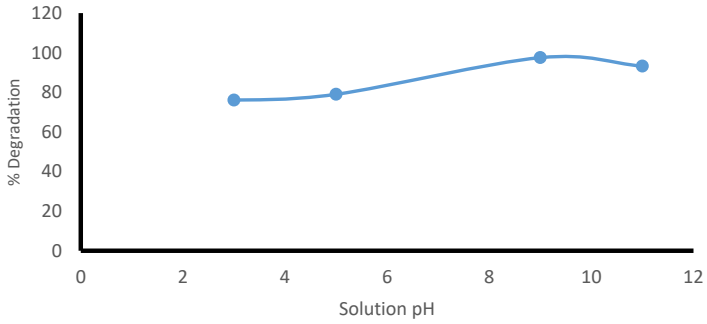

Figure 8.0: Effect of solution pH on degradation of MB

Effect of photocatalyst dosage on degradation of MB dye

The effect of photocatalyst dosage plays a significant role in Photocatalysis as it is vital for the optimization of materials in wastewater treatment. In this research, the effect of photocatalyst dosage at constant pH of 9, time of 75 minutes and constant initial concentration of 10 mg/L was studied.

From Figure 6, it is observed that there is a continuous increase in percentage degradation of MB dye as photocatalyst dosage increase until the photocatalyst dosage exceeded 100 mg. Further increase of photocatalyst dosage beyond 100 mg resulted in a decrease in percentage degradation. This may be attributed to the agglomeration of photocatalyst particles in the solution, increase in turbidity of the solution, which induce a reduction in light penetration.

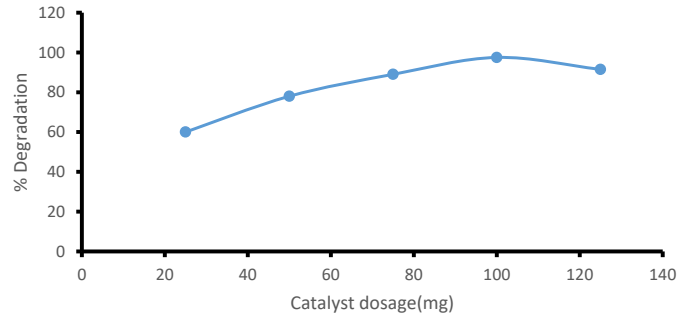

Figure 9.0: Effect of photocatalyst dosage on degradation of MB dye

Effect of initial concentration of MB dye solution

The changes in effluent concentration from the textile industry made it imperative to study the effect of initial concentration on percentage degradation. The effect of concentrations of MB dye solution at constant photocatalyst dosage of 100 mg, solution pH of 9 and time of 90 minutes was studied. From Figure 5, one can notice that percentage ceased to after 90 minutes and initial concentration of 5 mg/L had highest degradation. From this, we can deduce that percentage degradation decreases as the initial concentration of organic pollutants increases. This phenomenon can be attributed to increase in dye sorbate o the surface-active sites of the photocatalyst, thereby limiting adsorption of OH- which leads reduced formation of highly oxidative OH* radicals. Also, higher dye concentration reduces visible light penetration on the surface of and active sites of the photocatalyst thus reducing the activity of the photocatalyst. Vasiljevic (2020).

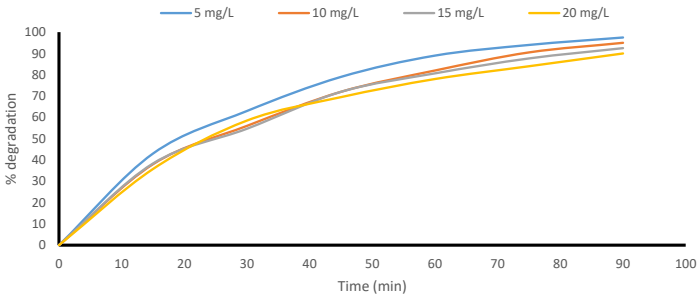

Figure 10: Effect of initial concentration on degradation of MB dye

Data fitting and Model Validation

Python Programming Language (Scipy, Numpy, Pandas and Matplotlib libraries) was used to perform data fittings and model validation for this research. The lines of codes/scripts below describe steps followed. The experimental data (concentration vs time) was fitted on the first, second and third order kinetic equations. First order kinetic equations had the best fittings as shown in Figure 8, 9, and 10 below, hence it was adopted for the kinetic studies.

a. Data fitting and model validation (1ST, 2ND & 3RD order kinetics)

```
# Importing Python Libraries; Numpy, Scipy, Matplotlib
import numpy as np
from scipy.optimize import minimize
import matplotlib.pyplot as plt
# Creating variables; Ca is experimental concentration and T is time in minutes
Cao = 5.0
Ca = np.array([5,2.85,1.85,1.05,0.55,0.3,0.125])
T = np.array([0,15,30,45,60,75,90])

# Defining a function
def kine(k,t,c):
 Ca_cal = np.zeros(len(Ca))
 for i in range(0, len(Ca)):
 Ca_cal[i] = Cao*(np.exp(-k*T[i]))
 res = Ca_cal - Ca
 SSE = sum(res**2)
 return SSE

#Minimize function
OPM = minimize(kine,0,,args=(T,Ca))
k = OPM.x
```

```
# Reevaluation of parameters
Ca_cal = np.zeros(len(Ca))
for i in range(0, len(Ca)):
 Ca_cal[i] = Cao*(np.exp(-k*T[i]))

#Creating Plots
plt.plot(T,Ca_cal,linewidth=2,color='b')
plt.scatter(T,Ca,color="r")
plt.xlabel("Time (Min)")
plt.ylabel("Concentration (mg/L")
plt.title("Data Fitting: 1st order Kinetics")
plt.legend(["Estimated Ca from 1st order kinetics", "Experimental Ca"])
plt.show()
```

Similarly, the lines of code are repeated for 2ND and 3RD order kinetic equations by replacing Ca_cal[i] = Cao*(np.exp(-k*T[i])) with Ca_cal[i] = Cao/(1+Cao*(k)*(T[i])) and Ca_cal[i] = Cao*(np.exp(-k*T[i])) with Ca_cal[i] = (Cao**2/(1+2*(Cao**2)*(k)*(T[i])))**(1/2) respectively.

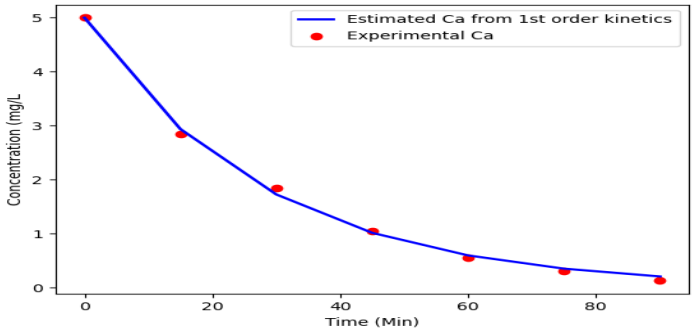

Figure 11: Experimental and Estimated data fitting for 1ST order Kinetic equation

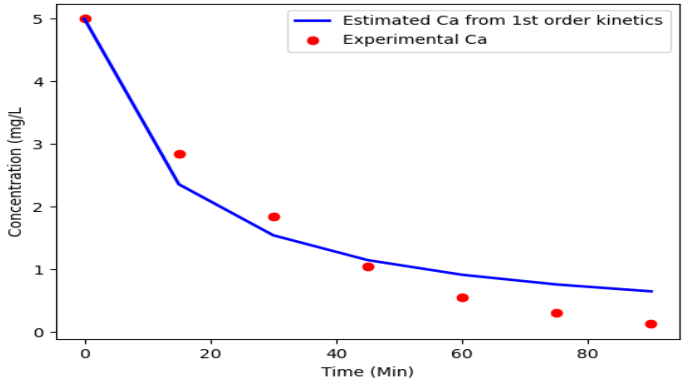

Figure 12: Experimental and Estimated data fitting for 2ND order Kinetic equation

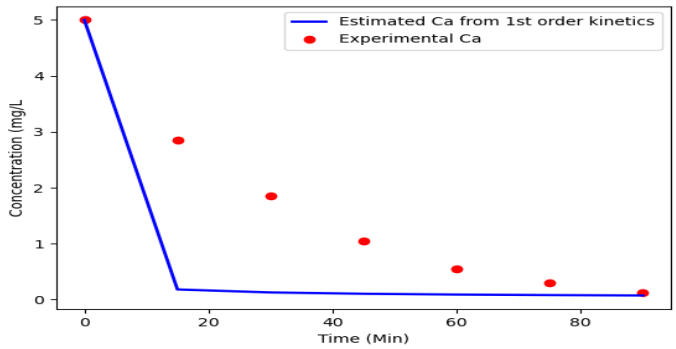

Figure 13: Experimental and Estimated data fitting for 3RD order Kinetic equation

Reaction kinetics

The rate of degradation of MB dye was studied with the first order kinetics using the kinetic expression below;

$$\ln (Cao/Ca) = K * t. \quad (1)$$

Where KC = rate constant and Cao = initial concentration and Ca = concentration at time t.

Figure 11 presents a linear plot of ln (C_{ao}/C_a) against time. The slope of each linear represents the rate constants (Kc) initial concentrations. The Kc values for 5, 10, 15 and 20 mg/L initial concentrations are 0.04 min^{-1}, 0.0325 min^{-1}, 0.0282 min^{-1} and 0.0246 min^{-1} respectively.

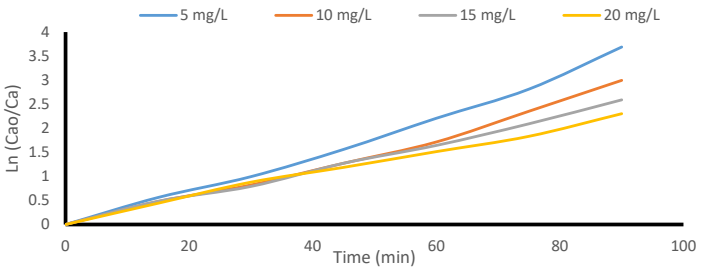

Figure 14: Plot of ln (Cao/Ca) vs time

Table 3: Rate constant (K) and correlation coefficients (R^2)

C_a (mg/L)	Linear equation	(K_C)	R^2
5	y = 0.04x – 0.1086	0.04	0.9906
10	y = 0.0325x - 0.084	0.0325	0.9888
15	y = 0.0282x - 0.0011	0.0282	0.9976
20	y = 0.0246x - 0.0595	0.0246	0.9955

Sum of square error (SSE) analysis

res = c_cal - c
*SSE = sum(res**2)*
Print(c_cal)
print(res)
print(SSE)

Where Ca_cal = estimated Ca, Ca = experimental Ca, t = time, SSE = sum of square errors and Cao = Initial concentration

Table 4: Sum of Square Error (SSE) Analysis

Time (min)	Experimental Ca	Estimated Ca	Absolute Error |E|	E^2
0	5.00	5.00	0	0
15	2.85	2.94	0.09	0.0081
30	1.85	1.72	0.13	0.0169
45	1.05	1.01	0.04	0.0016
60	0.55	0.59	0.04	0.0016
75	0.3	0.35	0.05	0.0025
90	0.125	0.21	0.085	0.007225
				Σ of E^2 = 0.037925

Proposed reaction mechanism

The following reactions represents the proposed reaction mechanism for the photocatalytic degradation of methylene blue dye with green synthesized nitrogen doped zinc oxide.

1.Absorption of efficient photons (hv≥EG=3.2 eV) by green synthesized nitrogen doped zinc oxide

N-ZnO + hv ⟶ e-CB + h+VB
(Photocatalyst) (Photon)

2. Oxygen ionosorption (first step of oxygen reduction; oxygen's oxidation from 0 to −1/2)

(O2) ads + e-CB ⟶ O_2o-

3. Neutralization of OH− groups by photo-holes which produces OH◦ radicals

(H2O) ads + h+VB ⟶ H^+ + OH◦

4. Neutralization of O2o- by protons

O_2o- + H^+ ⟶ HO_2o-

5. Transient hydrogen peroxide formation and dismutation of oxygen

2HO_2o- ⟶ H_2O_2 + O_2

6. Decomposition of H_2O_2 and second reduction of oxygen

H_2O_2 + e- ⟶ OH◦ + OH-

7. Oxidation of the organic reactant via successive attacks by OH◦ radicals

R + OH◦ ⟶ R• + H2O
(akyl group)

8. Direct oxidation by reaction with holes

R + h+ ⟶ R+◦ degradation products

9. A case of step 8 involves holes can reacting directly with carboxylic acids and generating carbon dioxide

RCOO- + h+ R• + CO2

Conclusion

The synthesis of pure zinc oxide and green synthesized nitrogen doped zinc oxide (G. S N-ZnO) from zinc nitrate hexahydrate, urea and paw-paw plants liquid extract has been carried out in this research. The morphology, functional groups, surface properties and crystallinity of pure ZnO and G. S N-ZnO were studied through SEM-EDX, FTIR, BET and XRD analysis. The distinct

difference in results from SEM-EDX, FTIR, BET and XRD analysis for pure ZnO and G. S N-ZnO confirms that doping and green synthesis were successfully performed during the photocatalyst preparation stage. The effects of process parameters such as: solution pH, photocatalyst dosage and initial concentration of MB dye solution on degradation of MB dye with G. S N-ZnO were studied. Optimum percentage degradation of MB with pure ZnO and G. S N-ZnO at the same process conditions (solution pH of 9.0, photocatalyst dosage of 100 mg and Initial concentration of 10 mg/L) were 83% and 97.5% respectively. The results obtained from this study revealed that doping and green synthesis had significant positive effect on the photocatalytic capability of zinc oxides and consequently increases degradation of MB dye. In addition, this research has demonstrated that degradation of organic pollutants in the presence of sunlight during wastewater treatment is economically viable, and could be deployed in large wastewater treatment systems [1-40].

References

1. Ahmad, A., Jini, D., Aravind, M., Parvathiraja, C., Ali, R., Kiyani, M. Z., & Alothman, A. (2020). A novel study on synthesis of egg shell based activated carbon for degradation of methylene blue via photocatalysis. Arabian Journal of Chemistry, 13(12), 8717-8722.
2. Akpan, U. G., & Hameed, B. H. (2009). Parameters affecting the photocatalytic degradation of dyes using TiO2-based photocatalysts: a review. Journal of hazardous materials, 170(2-3), 520-529
3. Aljuboury, D. A. D. A., Palaniandy, P., Abdul Aziz, H. B., & Feroz, S. (2017). Degradation of total organic carbon (TOC) and chemical oxygen demand (COD) in petroleum wastewater by solar photo-Fenton process. Glob. NEST J, 19, 430-438.
4. Ali, N., Ali, F., Sheikh, Z. A., Bilal, M., & Ahmad, I. (2020). Photocatalytic performance of zinc ferrite magnetic nanostructures for efficient eriochrome black-T degradation from the aqueous environment under unfiltered sunlight. Water, Air, & Soil Pollution, 231(2), 1-12.
5. Aminuzzaman, M., Ng, P. S., Goh, W. S., Ogawa, S., & Watanabe, A. (2019). Value-adding to dragon fruit (Hylocereus polyrhizus) peel biowaste: green synthesis of ZnO nanoparticles and their characterization. Inorganic and Nano-Metal Chemistry, 49(11), 401-411.
6. Amita K, & Rana, P. S. (2019). Visible light photocatalysis of methylene blue using cobalt substituted cubic NiO nanoparticles. Bulletin of Materials Science, 42(4), 1-11.
7. Ahmad, A., Jini, D., Aravind, M., Parvathiraja, C., Ali, R., Kiyani, M. Z., & Alothman, A. (2020). A novel study on synthesis of egg shell based activated carbon for degradation of methylene blue via photocatalysis. Arabian Journal of Chemistry, 13(12), 8717-8722.
8. Chen, L., Wang, L., Wu, X., & Ding, X. (2017). A process-level water conservation and pollution control performance evaluation tool of cleaner production technology in textile industry. Journal of cleaner production, 143, 1137-1143.
9. Cotillas, S., Llanos, J., Cañizares, P., Clematis, D., Cerisola, G., Rodrigo, M. A., & Panizza, M. (2018). Removal of Procion Red MX-5B dye from wastewater by conductive-diamond electrochemical oxidation. Electrochimica Acta, 263, 1-7.
10. Mortezaali, A., & RamezaniSani, S. (2019). Visible light photocatalytic activity of MWCNT/TiO2 using the degradation of methylene blue. Journal of Interfaces, Thin Films and Low dimensional systems, 2(2), 149-156.
11. Dhanalakshmi, M., Saravanakumar, K., Prabavathi, S. L., & Muthuraj, V. (2020). Iridium doped ZnO nanocomposites: synergistic effect induced photocatalytic degradation of methylene blue and crystal violet. Inorganic Chemistry Communications, 111, 107601.
12. Din, M. I., Jabbar, S., Najeeb, J., Khalid, R., Ghaffar, T., Arshad, M. & Ali, S. (2020). Green synthesis of zinc ferrite nanoparticles for Photocatalysis of methylene blue. International Journal of Phytoremediation, 22(13), 1440-1447.
13. Kaliraj, L., Ahn, J. C., Rupa, E. J., Abid, S., Lu, J., & Yang, D. C. (2019). Synthesis of panos extract mediated ZnO nano-flowers as photocatalyst for industrial dye degradation by UV illumination. Journal of Photochemistry and Photobiology B: Biology, 199, 111588.
14. Kanan, S., & Samara, F. (2018). Dioxins and furans: A review from chemical and environmental perspectives. Trends in Environmental Analytical Chemistry, 17, 1-13.
15. Khairnar, S. D., & Shrivastava, V. S. (2019). Facile synthesis of nickel oxide nanoparticles for degradation of methylene blue and Rhodamine B dye: a comparative study. Journal of Taibah University for Science, 13(1), 1108-1118.
16. Khatri, A., & Rana, P. S. (2019). Visible light Photocatalysis of methylene blue using cobalt substituted cubic NiO nanoparticles. Bulletin of Materials Science, 42(4), 1-11.
17. Kumar, J. S., Bolimera, U. R., & Thangadurai, P. (2019, July). Direct sunlight responsive ZnO photocatalyst: Highly efficient photodegradation of methylene blue. In AIP Conference Proceedings (Vol. 2115, No. 1, p. 030080). AIP Publishing LLC.
18. Kwon, D., & Kim, J. (2020). Silver-doped ZnO for photocatalytic degradation of methylene blue. Korean Journal of Chemical Engineering, 37(7), 1226-1232.
19. Lawal, A. T. (2017). Polycyclic aromatic hydrocarbons. A review. Cogent Environmental Science, 3(1), 1339841.
20. Marques, J., Gomes, T. D., Forte, M. A., Silva, R. F., and Tavares, C. J. (2019). A new route for the synthesis of highly-active N-doped TiO2 nanoparticles for visible light photocatalysis using urea as nitrogen precursor. Catalysis Today, 326, 36-45.
21. Megharaj, M., Ramakrishnan, B., Venkateswarlu, K., Sethunathan, N., & Naidu, R. (2011). Bioremediation approaches for organic pollutants: a critical perspective. Environment international, 37(8), 1362-1375.
22. Messih, M. A., Ahmed, M. A., Soltan, A., & Anis, S. S. (2019). Synthesis and characterization of novel Ag/ZnO nanoparticles

for photocatalytic degradation of methylene blue under UV and solar irradiation. Journal of Physics and Chemistry of Solids, 135, 109086.
23. M. Golmohammadi, M. Honarmand and S. Ghanbari. (2019). A green approach to synthesis of ZnO nanoparticles using jujube fruit extract and their application in photocatalytic degradation of organic dyes, Spectrochimica Acta Part A: Molecular and Biomolecular Spectroscopy.
24. Muhammad Imran Din, Summiya Jabbar, Jawayria Najeeb, Rida Khalid, Tayabba Ghaffar, Muhammad Arshad, Safyan A. Khan & Shahid Ali. (2020). Green synthesis of zinc ferrite nanoparticles for degradation of methylene blue dye, International Journal of Phytoremediation.
25. Nguyen, C. H., Fu, C. C., & Juang, R. S. (2018). Degradation of methylene blue and methyl orange by palladium-doped TiO2 photocatalysis for water reuse: Efficiency and degradation pathways. Journal of Cleaner Production, 202, 413-427.
26. Osuntokun, J., Onwudiwe, D. C., & Ebenso, E. E. (2019). Green synthesis of ZnO nanoparticles using aqueous Brassica oleracea L. var. italica and the photocatalytic activity. Green Chemistry Letters and Reviews, 12(4), 444-457.
27. Pai, S., Sridevi, H., Varadavenkatesan, T., Vinayagam, R., & Selvaraj, R. (2019). Photocatalytic zinc oxide nanoparticles synthesis using Peltophorum pterocarpum leaf extract and their characterization. Optik, 185, 248-255.
28. Prabakaran, E., & Pillay, K. (2019). Synthesis of N-doped ZnO nanoparticles with cabbage morphology as a catalyst for the efficient photocatalytic degradation of methylene blue under UV and visible light. RSC Advances, 9(13), 7509-7535.
29. Rajagopal, S., Paramasivam, B., & Muniyasamy, K. (2020). Photocatalytic removal of cationic and anionic dyes in the textile wastewater by H2O2 assisted TiO2 and micro-cellulose composites. Separation and Purification Technology, 252, 117444.
30. Rauwel, P., Küünal, S., Ferdov, S., & Rauwel, E. (2015). A review on the green synthesis of silver nanoparticles and their morphologies studied via TEM. Advances in Materials Science and Engineering, 2015.
31. Rowshon K., Saifullah, M., Khalid, A., Ahmed, A. Z., Masum, S. M., Molla, M., & Islam, A. (2020). Synthesis of N-Doped ZnO Nanocomposites for Sunlight Photocatalytic Degradation of Textile Dye Pollutants. Journal of Composites Science, 4(2), 49.
32. Saravanakumar T, M., Newman, J. P., & Kubheka, O. (2020). Effect of TiO2 phase on the photocatalytic degradation of methylene blue dye. Physics and Chemistry of the Earth, Parts A/B/C, 118, 102900.
33. Sinar Mashuri, S. I., Ibrahim, M. L., Kasim, M. F., Mastuli, M. S., Rashid, U., Abdullah, A. H., ... & Yun
34. Hin, T. Y. (2020). Photocatalysis for organic wastewater treatment: From the basis to current challenges for society. Catalysts, 10 (11), 1260.
35. Subbiah, R., Muthukumaran, S., & Raja, V. (2019). Fine-tuning of energy gap, FTIR, photoluminescence and photocatalytic behavior of Centella asiatica extract mediated Mn/Mg doped ZnO nanostructure. Journal of Materials Science: Materials in Electronics, 30 (18), 17066-17077.
36. Sun, L., Shao, Q., Zhang, Y., Jiang, H., Ge, S., Lou, S., & Guo, Z. (2020). N self-doped ZnO derived from microwave hydrothermal synthesized zeolitic imidazolate framework-8 toward enhanced photocatalytic degradation of methylene blue. Journal of colloid and interface science, 565, 142-155.
37. Ullah, A. A., Kibria, A. F., Akter, M., Khan, M. N. I., Tareq, A. R. M., & Firoz, S. H. (2017). Oxidative degradation of methylene blue using Mn 3 O 4 nanoparticles. Water Conservation Science and Engineering, 1(4), 249-256.
38. Varadavenkatesan, T., Lyubchik, E., Pai, S., Pugazhendhi, A., Vinayagam, R., & Selvaraj, R. (2019). Photocatalytic degradation of Rhodamine B by zinc oxide nanoparticles synthesized using the leaf extract of Cyanometra ramiflora. Journal of Photochemistry and Photobiology B: Biology, 199, 111621.
39. Vasiljevic, Z. Z., Dojcinovic, M. P., Vujancevic, J. D., Jankovic-Castvan, I., Ognjanovic, M., Tadic, N. B and Nikolic, M. V. (2020). Photocatalytic degradation of methylene blue under natural sunlight using iron titanate nanoparticles prepared by a modified sol–gel method. Royal Society open science, 7(9), 200 and 708.
40. Vermorel, N., San-Valero, P., Izquierdo, M., Gabaldón, C., & Penya-Roja, J. M. (2017). Anaerobic degradation of 2-propanol: Laboratory and pilot-scale studies. Chemical Engineering Science, 172, 42-51.
41. Wang, W., Tadé, M. O., & Shao, Z. (2018). Nitrogen-doped simple and complex oxides for photocatalysis: a review. Progress in Materials Science, 92, 33-63.